Catalysis Science & Technology

ROYAL SOCIETY OF CHEMISTRY

PAPER

View Article Online
View Journal | View Issue

Cite this: *Catal. Sci. Technol.*, 2023, 13, 2994

Multi-functionality of rhodium-loaded MOR zeolite: production of H_2 *via* the water gas shift reaction and its use in the formation of NH_3†

Shunsaku Yasumura, [a] Ken Nagai,[a] Yucheng Qian,[a] Takashi Toyao, [a] Zen Maeno [b] and Ken-ichi Shimizu *[a]

Rh-loaded mordenite (RhMOR) zeolite was investigated as a catalyst that can use CO + H_2O as a H_2 source for NO reduction. *Operando* IR measurements showed that CO was captured in the form of Rh dicarbonyl species ($[Rh(CO)_2]^+$) in zeolite, which reacts with H_2O to form H_2 *in situ via* the water gas shift (WGS) reaction (CO + H_2O → CO_2 + H_2) at >350 °C. Temperature-programmed surface reaction (TPSR) measurements under a flow of NO + CO + H_2O monitored both the surface ad-species and outlet gas components. At >250 °C, the decrease in the outlet NO and CO as well as the increase in the IR intensity corresponding to NH_4^+ in zeolite were observed, indicating that the formed H_2 was directly used for the reduction of NO into NH_3, which was stored at the Brønsted acid sites (BAS). The mechanism of the WGS reaction was theoretically investigated; the predicted rate-determining step was the dissociation of H_2O on $[Rh(CO)_2]^+$ to give $[Rh(CO)(COOH)(H)]^+$ and its activation barrier was 176 kJ mol^{-1}. The present study demonstrates the effective use of the multi-functionality of the isolated active metal anchored in zeolite as well as the potential utilization of CO + H_2O as a H_2 source.

Received 10th January 2023,
Accepted 16th April 2023

DOI: 10.1039/d3cy00043e

rsc.li/catalysis

1. Introduction

Atomically dispersed noble metals on solid supports, known as single-atom catalysts (SACs), have attracted a significant amount of attention because they provide the maximum utilization of expensive metals.[1–3] Among the various supporting materials used for isolated metal catalysts, crystalline supports such as zeolites offer nearly uniform anchoring sites for the isolated metals, resulting in the formation of nearly uniform supported metal complexes.[4–8] Much research effort has been devoted to obtaining molecular-level insight into the structure and reactivity of the metal complexes in zeolites.[9–16] Rhodium complexes anchored in zeolites, as representative examples of well-defined active species,[17–22] have been studied using *in situ*/*operando* spectroscopic techniques and density functional theory (DFT) calculations in order to identify the changes in their coordination environment during their reaction with small molecules.[4–8,23–27] The group of Amiridis conducted X-ray absorption spectroscopy (XAS), high-resolution scanning transmission electron microscopy (HRSTEM), infrared (IR), and density function theory (DFT) calculations to clarify the detailed structure of the isolated $[Rh(NO)_2]^+$ complexes in zeolite and their catalytic activity toward the hydrogenation and dimerization of hydrocarbons.[21] Although previous reports have studied model reactions over the Rh complexes in zeolites, only a few studies have focused on practical catalytic reactions under unsteady-state conditions driven by the reversible structural changes in the Rh complexes.[23]

The use of CO + H_2O as reductant to reduce NO to NH_3 was proposed in the previous papers.[28–44] The group of Christopher[45] and that of Wang[46] independently reported that atomically dispersed (single atom) Rh sites on Al_2O_3 and CeO_2 exhibit high selectivity toward NH_3 in the NO + CO + H_2O reaction. These studies suggest that single-atom Rh sites catalyze the formation of NH_3 *via* the reduction of NO using H_2 produced by the water gas shift (WGS) reaction (CO + H_2O → H_2 + CO_2). Inspired by the pioneering works by Nakatsuji and co-workers,[47] we have reported an unsteady-state NO_x reduction system using a Rh-loaded zeolite catalyst. The method is based on a two-step cyclic operation, in which the NO_x trapped on the catalyst during the lean period is reduced by H_2 to form NH_3 during rich period (fuel-rich condition). Based on the *operando* spectroscopic and DFT results, it has been found that the reduction of the $[Rh(NO)_2]^+$ complexes

[a] *Institute for Catalysis, Hokkaido University, N-21, W-10, Sapporo 001-0021, Japan. E-mail: kshimizu@cat.hokudai.ac.jp*
[b] *School of Advanced Engineering, Kogakuin University, 2665-1 Nakano-cho, Hachioji, Tokyo 192-0015, Japan*

† Electronic supplementary information (ESI) available: The experimental and theoretical details as well as the additional data of IR spectra and DFT calculation are included. See DOI: https://doi.org/10.1039/d3cy00043e

by H_2 results in NH_3 as an intermediate, which then reduces NO_x to give N_2.[48,49]

In this study, we have conducted IR experiments and DFT calculations for Rh-loaded mordenite zeolite (Rh-MOR) with a low Rh loading. *Operando* IR experiments were carried out using transient or temperature-programed surface reaction (TPSR) measurements. The results obtained under a flow of CO + H_2O show that CO was captured in the form of $[Rh(CO)_2]^+$ complex, which reacts with H_2O to produce CO_2 + H_2 *via* the WGS reaction at >350 °C. In the presence of NO, the H_2 formed *in situ* (*via* the WGS reaction) was directly used for the reduction of NO to form NH_3 at >250 °C. Transition state calculations confirmed that the Rh cation was practical as the active site for the WGS reaction.

2. Results and discussion

2.1. TPSR and *operando* IR studies on the WGS reaction and NH_3 formation

To assess the effect of temperature on the WGS reaction, CO + H_2O was fed to 0.6 wt% Rh-loaded MOR zeolite (RhMOR) under temperature-ramping conditions. RhMOR was prepared *via* the aqueous ion-exchange method using NH_4^+ – MOR (Si/Al = 10) with the aqueous solution of $RhCl_3$ (see ESI†). The catalyst was subjected to CO + H_2O at room temperature and heated to 500 °C at a ramping rate of 20 °C min^{-1}. The concentration of CO and CO_2 in the outlet gas was analyzed using IR (gas cell) and the relative concentration of H_2 was estimated using mass spectrometry (MS). The outlet gas profile (Fig. 1) shows that CO_2 was observed at >250 °C and its formation rate increases at >400 °C. H_2 evolution was observed at >350 °C. Since the fed H_2O is the only source of hydrogen atoms, these results indicate that the WGS reaction was catalyzed by RhMOR at >350 °C. The consecutive mechanism of the WGS on RhMOR will be discussed based on our DFT calculations.

The mechanism of the WGS reaction over RhMOR was examined by TPSR measurements using *in situ* IR measurements of the adsorbed species combined with online IR and MS analyses of the effluent gas (*operando* IR). A schematic representation of the setup used is shown in Fig. S1.† The catalyst powder was pelletized into a self-supported IR disk (40 mg) and set in the *in situ* IR cell. The concentration of CO_2 in the outlet gas was monitored using another IR equipped with an IR gas cell, while the evolution of H_2 was monitored by MS. The IR disk was first pretreated under a flow of 2% O_2 at 350 °C and then subjected to a flow of 0.5% CO/He at 200 °C. Fig. 2(left) shows the IR spectra of CO adsorbed on RhMOR. According to the literature,[7,19,23] the two characteristic IR peaks observed at 2044 cm^{-1} and 2108 cm^{-1} can be ascribed to the isolated dicarbonyl Rh^+ complexes ($[Rh(CO)_2]^+$) stabilized at the Al sites in the zeolite. After purging with He, the disk was further subjected to a flow of 1% H_2O/He at 350 °C. Upon exposure to H_2O, the intensity of the IR peaks corresponding to $[Rh(CO)_2]^+$ decreased and were scarcely observed after 600 s of exposure. Note that the formation of $[Rh(CO)]^+$ was not observed here as discussed in the previous report which revealed that the desorption of the second CO is rapid at high temperatures using *in situ* IR spectroscopy.[50] The time course of the concentration of CO_2 as well as the MS intensity of H_2 in the outlet gas are plotted in Fig. 2(right) together with the IR intensity at 2044 cm^{-1} for $[Rh(CO)_2]^+$. When H_2O was fed to the CO adsorbed RhMOR, the IR intensity of the $[Rh(CO)_2]^+$ complex decreased, and the concentration of CO_2 and MS intensity of H_2 in the outlet gas increased. This indicates that CO coordinated to the Rh^+ sites ($[Rh(CO)_2]^+$ complex) react with H_2O to give CO_2 and H_2 (*i.e.* the WGS reaction).

Recently, we reported that RhMOR catalyzed the selective formation of NH_3 from NO + H_2 and the subsequent capture of *in situ* formed NH_3 at the Brønsted acid sites (BASs) in the zeolite. Aiming at H_2 formation from CO and H_2O, followed by NH_3 formation from NO + H_2, we conducted TPSR in combination with *operando* IR measurements under a flow of NO + CO + H_2O over RhMOR. The TPSR profile shows the formation of CO_2 at >250 °C (Fig. 3). The concentration of CO_2 (*i.e.* relative rate of CO_2 formation) in a temperature range of 300–500 °C under NO + CO + H_2O was higher than that observed under CO + H_2O (Fig. 1) due to the competitive NO + CO reaction. In the IR spectra obtained for the adsorbed species, the NH_3 adsorbed on the BASs in MOR (NH_4^+) was observed at >250 °C (Fig. S2†), while gaseous NH_3 was observed in outlet gas at >350 °C. Compared to the formation of gaseous H_2 in NO + H_2O flow (Fig. 1), the temperature of NH_3 formation is lower (<250 °C *vs.* <350 °C). These results suggest that the H_2 formed *in situ* (*via* the WGS reaction over RhMOR) acts as a reductant to reduce NO to form NH_3.

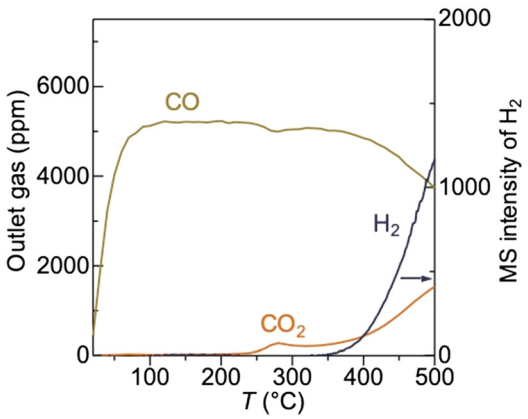

Fig. 1 MS intensity of H_2 (arbitrary unit) and the concentration of CO and CO_2 (ppm) during ramping the temperature (20 °C min^{-1}) under a flow of 0.5% CO + 1% H_2O over RhMOR.

2.2. DFT study on the WGS mechanism over the Rh^+ cation in MOR zeolite

Reaction route mapping, as implemented in the GRRM17 program,[51] based on DFT calculations within periodic boundary condition was performed to investigate the mechanism of the WGS reaction over the RhMOR catalyst. The isolated $[Rh(CO)_2]^+$

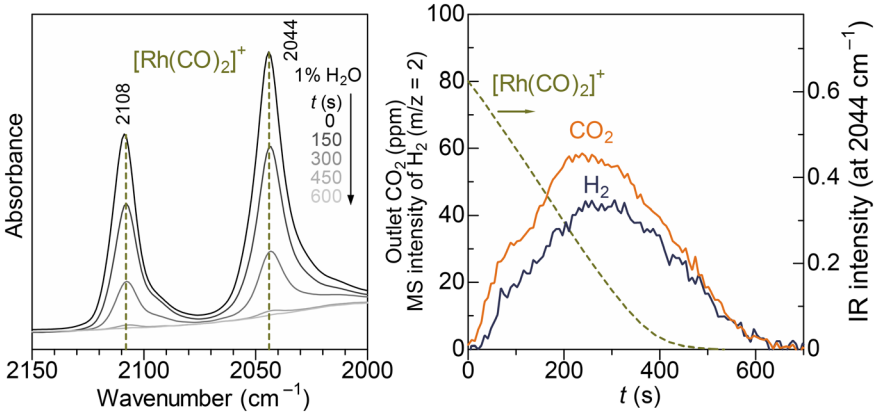

Fig. 2 The changes in the *in situ* IR spectra obtained for $[Rh(CO)_2]^+$ in RhMOR under a flow of 1% H_2O at 350 °C (left), the time course of the height of the IR peak for $[Rh(CO)_2]^+$, and MS intensity (arbitrary unit) of H_2 and CO_2 (right). The IR disk was pre-exposed to 0.5% CO at 200 °C (600 s), followed by purging with He (600 s).

species, which were observed under a flow of CO using *in situ* IR (Fig. 2), was used as the initial structure. Among the distinct T sites in MOR zeolite, the T4 site was applied as the Al replacement site (Fig. 4a). Note that MOR framework comprises four crystallographically inequivalent T sites; among them, T4 site is known as the energetically preferred Al replacement site. Assuming that one-fourth of the Al sites are T4 sites, the Rh/Al_{T4} ratio is calculated to be 0.14, which suggests that there are ample T4 sites available to accommodate Rh cations.[52,53] Fig. 4b shows the reaction pathway for the $Rh(CO)_2$ species with a H_2O molecule weakly bound to the zeolite framework. In the calculated reaction, two pathways were investigated as the initial steps: (i) The adsorption of H_2O onto the $Rh(CO)_2$ species to give $Rh(CO)_2(H_2O)$ and (ii) the dissociative adsorption of H_2O to give Rh(CO)(COOH)(H) species. Although the former pathway proceeds *via* a low activation barrier (38 kJ mol^{-1}) as the first step, the following reaction requires a very high activation energy (370 kJ mol^{-1}) to produce the $Rh(CO)_2(OH)$ species and BAS. The latter pathway, which forms the Rh(CO)(COOH)(H) species *via* an activation barrier (176 kJ mol^{-1}) as the first step, subsequently forms a $Rh(CO)(H)_2$ species and CO_2 molecule. The formation of $Rh(CO)(H)_2$ species is previously reported over Rh-exchanged Y zeolite[17] and Rh-loaded Al_2O_3[54] by IR measurement under H_2 flow near room temperature. Fig. 5 shows the energy profile along with the reaction coordinate for the reaction of the $Rh(CO)_2$ species with H_2O. The result indicates that although the activation barrier of the first step was higher than that forming the BAS (38 *vs.* 176 kJ mol^{-1}), the second step requires an activation energy of only 87 kJ mol^{-1}, and the relative energy of the products ($Rh(CO)(H)_2 + CO_2$) was lower (72 kJ mol^{-1}) when compared to $Rh(CO)_2(OH)$ + BAS (125 kJ mol^{-1}). Therefore, the formation of the $Rh(CO)(H)_2$ complex and CO_2 molecule was determined as the plausible pathway for the reaction of $Rh(CO)_2$ with H_2O. The formed CO_2 was then easily desorbed with a desorption energy of only 23 kJ mol^{-1} (Fig. S3†).

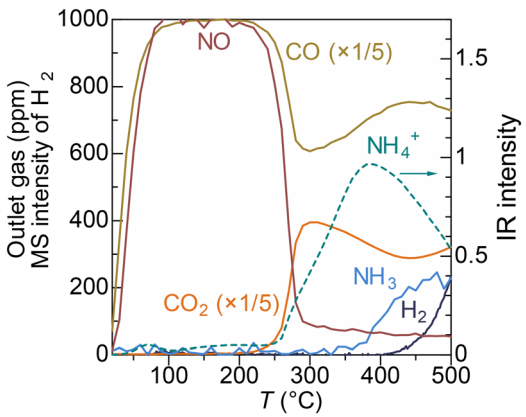

Fig. 3 The MS intensity of H_2 (arbitrary units), concentrations of NO, CO, and CO_2, and IR intensity of NH_4^+ during TPSR (20 °C min^{-1}) under a flow of 0.1% NO + 0.5% CO + 1% H_2O over RhMOR.

2.3. *Operando* IR measurements under periodic lean (NO + O_2 + H_2O)/rich (NO + CO + H_2O) conditions

Considering the presence of CO and water in the automotive exhaust gas and that Rh species can catalyze WGS reaction, we designed a two-stage de-NO_x method with RhMOR, where NH_3, formed *via* WGS followed by NO + H_2 reaction in rich (NO + CO + H_2O) period, is utilized as a reductant of NO_x in the subsequent lean (NO + O_2 + H_2O) period. Thus, *operando* IR measurements were carried out to observe the ad-species on the catalyst under periodic lean/rich conditions. The rich gas (0.1% NO + 0.5% CO + 1% H_2O; 300 s) and lean gas (0.1% NO + 2% O_2 + 1% H_2O; 600 s) were repeatedly fed into an *in situ* IR cell at 300 °C. Fig. 6 shows the representative IR spectra (left) and time course of outlet gases (NO, N_2O, CO, and CO_2) and IR intensities (B–NH_3 and NO_{ad}; right). Under lean conditions, the NO species adsorbed on the Rh cations (NO_{ad}) were observed at 1950 cm^{-1},[55,56] indicating that NO was captured by the catalyst. Under the subsequent rich conditions, the $[Rh(CO)_2]^+$ species and B–NH_3 appear in the IR spectra, while the peak corresponding to NO_{ad} was hardly detected. This observation

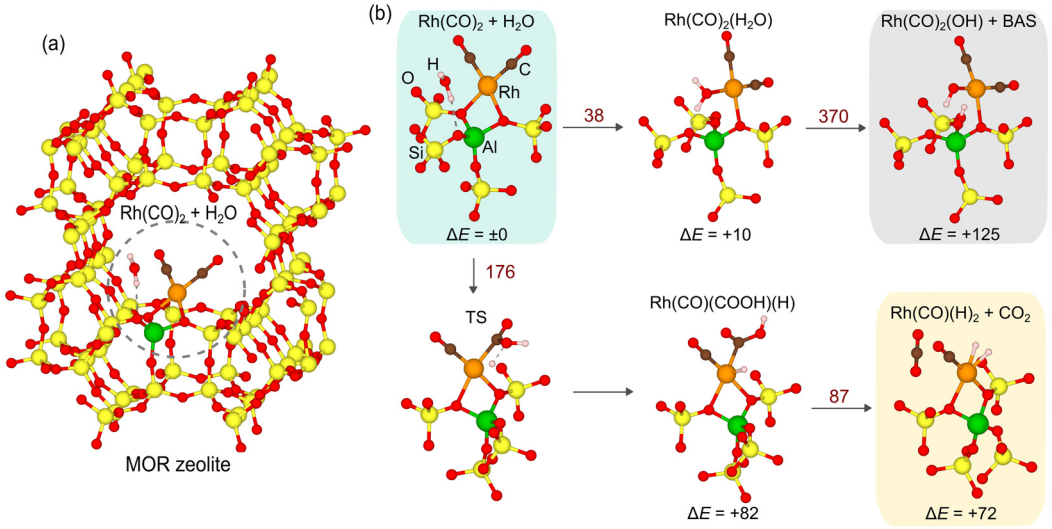

Fig. 4 (a) The periodic model used for MOR zeolite. (b) The calculated reaction pathway for $Rh(CO)_2$ and H_2O together with the relative energy (ΔE) values. The values written in dark red show the activation barrier. The relative energies are provided under each structure (units: kJ mol^{-1}).

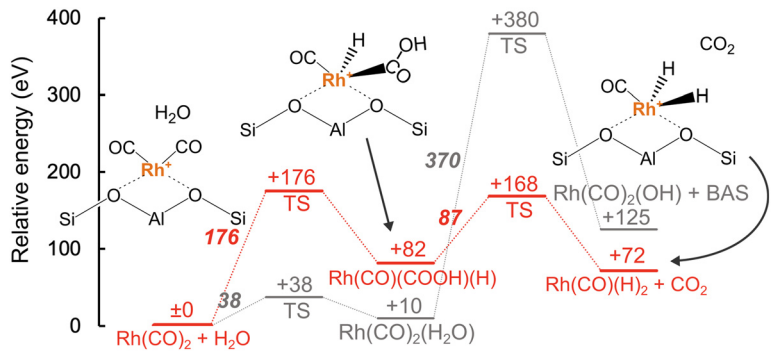

Fig. 5 Energy profile for the reaction of $Rh(CO)_2$ with water. The reaction pathway indicated by the red line is the most plausible pathway for CO_2 formation. The relative energies are provided under each bar and the activation barriers are shown using bold italic style (units: kJ mol^{-1}).

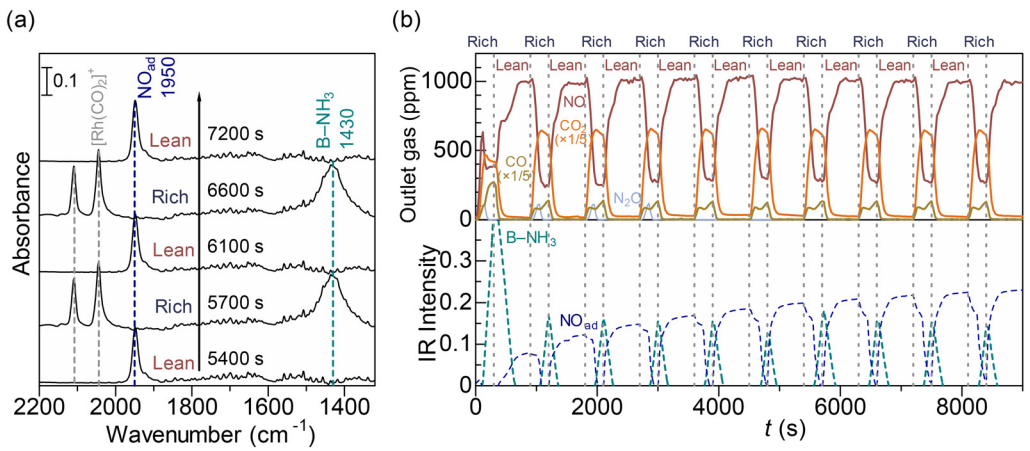

Fig. 6 (a) Representative IR spectra and (b) time course of outlet gases (NO, N_2O, CO, and CO_2) and IR intensities ($B–NH_3$ and NO_{ad}) obtained for the periodic rich (0.1% NO + 0.5% CO + 1% H_2O 300 s)/lean (0.1% NO + 2% O_2 + 1% H_2O; 600 s) conditions at 300 °C over Rh-MOR.

shows that Rh species in the zeolite are repeatably reduced back to isolated Rh species under the rich conditions while they were oxidized under the rich condition. We have confirmed that this process can be repeated at least 10 times (up to 9000 seconds)

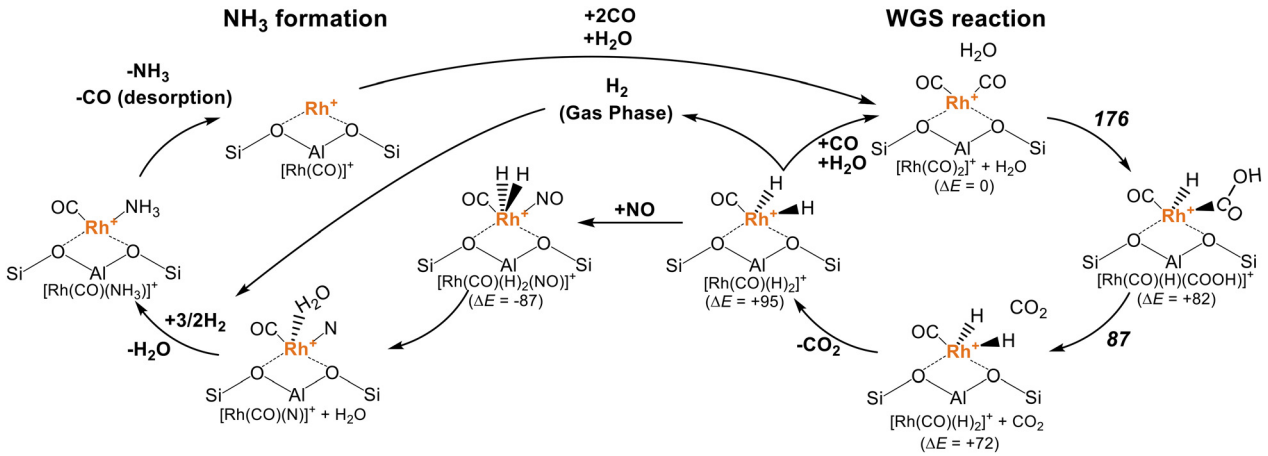

Fig. 7 The mechanism of the de-NO_x reaction using CO + H_2O with the RhMOR catalyst proposed in this study. The relative energies of each structure are shown together (ΔE). The activation barriers of the WGS reaction are shown in bold italic style. The reaction pathway for NH_3 formation was discussed in our previous report (unit: kJ mol^{-1}).[49]

without significant changes in performance. Note that the adsorbed NO (*e.g.* $Rh(NO)_2$) was not observed under rich conditions because the hydrogenation of NO required only 87 kJ mol^{-1} of the activation barrier as shown in our previous report.[49] The evaluated NO conversion and N_2 selectivity are 18% and 94%, respectively while gaseous NH_3 was not detected from the outlet gas (the products from the NO + CO reaction were possibly included). Combined with the TPSR measurements (Fig. 3), the H_2 formed *in situ* (*via* the WGS reaction) was used to reduce NO to form NH_3, which was then stored at the BASs in zeolite (B–NH_3).

Assuming that both the WGS reaction and NH_3 formation take place at the isolated Rh cations, their reaction mechanism can be described (Fig. 7). The WGS reaction occurs from $[Rh(CO)_2]^+ + H_2O$ to form $[Rh(CO)(H)_2]^+ + CO_2$ *via* activation barriers of 176 and 87 kJ mol^{-1}, respectively. After the desorption of CO_2, the resulting $[Rh(CO)(H)_2]^+$ complex follows two possible pathways: (i) the $[Rh(CO)_2]^+$ complex and adsorbed H_2O are recovered by the adsorption of CO and H_2O as well as the desorption of H_2, and (ii) the $[Rh(CO)(H)_2(NO)]^+$ complex was formed by the adsorption of NO. In the latter case, the adsorbed NO was reduced into a N atom and H_2O ($[Rh(CO)(H_2O)(N)]^+$), and then hydrogenated to form NH_3, as discussed in our previous study.[49,57–59] The consecutive stoichiometry is described as follows.

Rich condition:

$$2NO + 5CO + 3H_2O \rightarrow 2NH_3 + 5CO_2 \quad (1)$$

Lean condition (SCR reaction):

$$NO + NH_3 + \frac{1}{4}O_2 \rightarrow N_2 + \frac{3}{2}H_2O \quad (2)$$

The proposed reaction mechanism shows that the NO reduction using CO + H_2O as the reductant is driven by the multi-functionality of the anchored Rh cation that can catalyze both the WGS reaction and the formation of NH_3.

3. Conclusions

The NO reduction over RhMOR using CO + H_2O as reductants have been investigated by *in situ*/*operando* techniques and DFT calculations. TPSR measurements showed that the Rh species in zeolite can catalyze the WGS reaction (CO + H_2O → CO_2 + H_2O) *via* $[Rh(CO)_2]^+$ complex at >350 °C. Other TPSR measurements under 0.1% NO + 0.5% CO + 1% H_2O demonstrated the simultaneous formation of CO_2 and B–NH_3 at >250 °C, indicating that in the presence of NO, the H_2 formed *in situ* (*via* the WGS reaction) is directly used for the reduction of NO into NH_3 (B–NH_3). Our DFT calculations indicate that the rate-determining step of the WGS reaction is the dissociative adsorption of H_2O on $[Rh(CO)_2]^+$ to give a $[Rh(CO)(COOH)(H)]^+$ complex (175.6 kJ mol^{-1}). The present study has proposed the effective use of the multi-functionality of active metals anchored in zeolite as well as the potential utilization of CO + H_2O as reductants in the de-NO_x reaction.

Conflicts of interest

There are no conflicts to declare.

Acknowledgements

This research was financially supported by JSPS KAKENHI (21H04626). Some of the calculations were conducted employing the supercomputing resources at the Cyberscience Center of Tohoku University. This project was supported by the Joint Usage/Research Center for Catalysis. The authors would like to sincerely thank the Technical Division of the Institute for Catalysis at Hokkaido University.

References

1 A. Beniya and S. Higashi, *Nat. Catal.*, 2019, **2**, 590–602.
2 S. K. Kaiser, Z. Chen, D. Faust Akl, S. Mitchell and J. Pérez-Ramírez, *Chem. Rev.*, 2020, **120**, 11703–11809.

3 A. K. Datye and M. Votsmeier, *Nat. Mater.*, 2021, **20**, 1049–1059.
4 I. Ogino and B. C. Gates, *J. Phys. Chem. C*, 2010, **114**, 8405–8413.
5 P. Serna and B. C. Gates, *J. Am. Chem. Soc.*, 2011, **133**, 4714–4717.
6 P. Serna and B. C. Gates, *Angew. Chem., Int. Ed.*, 2011, **50**, 5528–5531.
7 C. Y. Fang, S. Zhang, Y. Hu, M. Vasiliu, J. E. Perez-Aguilar, E. T. Conley, D. A. Dixon, C. Y. Chen and B. C. Gates, *ACS Catal.*, 2019, **9**, 3311–3321.
8 J. E. Perez-Aguilar, C. Y. Chen, J. T. Hughes, C. Y. Fang and B. C. Gates, *J. Am. Chem. Soc.*, 2020, **142**, 11474–11485.
9 P. Rubio-Marqués, M. A. Rivero-Crespo, A. Leyva-Pérez and A. Corma, *J. Am. Chem. Soc.*, 2015, **137**, 11832–11837.
10 J. Cejka, A. Corma and S. Zones, *Zeolites and Catalysis*, Wiley, 2010.
11 S. Yasumura, H. Ide, T. Ueda, Y. Jing, C. Liu, K. Kon, T. Toyao, Z. Maeno and K. Shimizu, *JACS Au*, 2021, **1**, 201–211.
12 S. Yasumura, T. Ueda, H. Ide, K. Otsubo, C. Liu, N. Tsunoji, T. Toyao, Z. Maeno and K. Shimizu, *Phys. Chem. Chem. Phys.*, 2021, **23**, 22273–22282.
13 N. Kosinov, C. Liu, E. J. M. Hensen and E. A. Pidko, *Chem. Mater.*, 2018, **30**, 3177–3198.
14 M. H. Mahyuddin, Y. Shiota, A. Staykov and K. Yoshizawa, *Acc. Chem. Res.*, 2018, **51**, 2382–2390.
15 Z. Maeno, S. Yasumura, X. Wu, M. Huang, C. Liu, T. Toyao and K. Shimizu, *J. Am. Chem. Soc.*, 2020, **142**, 4820–4832.
16 G. Li and E. A. Pidko, *ChemCatChem*, 2019, **11**, 134–156.
17 K. Khivantsev, A. Vityuk, H. A. Aleksandrov, G. N. Vayssilov, O. S. Alexeev and M. D. Amiridis, *J. Phys. Chem. C*, 2015, **119**, 17166–17181.
18 T. T. T. Wong, A. Y. Stakheev and W. M. H. Sachtler, *J. Phys. Chem.*, 1992, **96**, 7733–7740.
19 E. Ivanova, M. Mihaylov, F. Thibault-Starzyk, M. Daturi and K. Hadjiivanov, *J. Catal.*, 2005, **236**, 168–171.
20 V. Markova, G. Rugg, A. Govindasamy, A. Genest and N. Rösch, *J. Phys. Chem. C*, 2018, **122**, 2783–2795.
21 K. Khivantsev, A. Vityuk, H. A. Aleksandrov, G. N. Vayssilov, D. Blom, O. S. Alexeev and M. D. Amiridis, *ACS Catal.*, 2017, **7**, 5965–5982.
22 W. Shang, M. Gao, Y. Chai, G. Wu, N. Guan and L. Li, *ACS Catal.*, 2021, 7249–7256.
23 C. Y. Fang, J. Valecillos, E. T. Conley, C. Y. Chen, P. Castaño and B. C. Gates, *J. Phys. Chem. C*, 2020, **124**, 2513–2520.
24 W. A. Weber and B. C. Gates, *J. Phys. Chem. B*, 1997, **101**, 10423–10434.
25 A. J. Dent, J. Evans, S. G. Fiddy, B. Jyoti, M. A. Newton and M. Tromp, *Angew. Chem., Int. Ed.*, 2007, **46**, 5356–5358.
26 Y. Kwon, T. Y. Kim, G. Kwon, J. Yi and H. Lee, *J. Am. Chem. Soc.*, 2017, **139**, 17694–17699.
27 S. Yasumura, T. Kato, T. Toyao, Z. Maeno and K. I. Shimizu, *Phys. Chem. Chem. Phys.*, 2023, 8524–8531.
28 K. Kobayashi, S. Ogawa, H. Matsumoto, K. Matsuda and T. Nanba, *J. Jpn. Pet. Inst.*, 2020, **63**, 28–37.
29 C. J. Yoo, A. Getsoian and A. Bhan, *Appl. Catal., B*, 2021, **286**, 119893.
30 K. Kobayashi, R. Atsumi, Y. Manaka, H. Matsumoto and T. Nanba, *Catal. Sci. Technol.*, 2019, **9**, 2898–2905.
31 E. C. Corbos, M. Haneda, X. Courtois, P. Marecot, D. Duprez and H. Hamada, *Catal. Commun.*, 2008, **10**, 137–141.
32 M. Sakai, T. Hamaguchi and T. Tanaka, *Appl. Catal., A*, 2019, **582**, 117105.
33 J. R. González-Velasco, B. Pereda-Ayo, U. De-La-Torre, M. Urrutxua and R. López-Fonseca, *ChemCatChem*, 2018, **10**, 2928–2940.
34 L. Castoldi, R. Bonzi, L. Lietti, P. Forzatti, S. Morandi, G. Ghiotti and S. Dzwigaj, *J. Catal.*, 2011, **282**, 128–144.
35 M. Kim, J. Choi and M. Crocker, *Catal. Today*, 2014, **231**, 90–98.
36 F. Can, X. Courtois, S. Royer, G. Blanchard, S. Rousseau and D. Duprez, *Catal. Today*, 2012, **197**, 144–154.
37 M. Urrutxua, B. Pereda-Ayo, L. V. Trandafilovic, L. Olsson and J. R. González-Velasco, *Ind. Eng. Chem. Res.*, 2019, **58**, 7001–7013.
38 M. Li, V. G. Easterling and M. P. Harold, *Appl. Catal., B*, 2016, **184**, 364–380.
39 S. H. Oh and T. Triplett, *Catal. Today*, 2014, **231**, 22–32.
40 V. Y. Prikhodko, J. E. Parks, J. A. Pihl and T. J. Toops, *Catal. Today*, 2016, **267**, 202–209.
41 K. Ramanathan, C. S. Sharma and C. H. Kim, *Ind. Eng. Chem. Res.*, 2012, **51**, 1198–1208.
42 C. D. Digiulio, J. A. Pihl, J. E. Parks, M. D. Amiridis and T. J. Toops, *Catal. Today*, 2014, **231**, 33–45.
43 M. Li, S. A. Malamis, W. Epling and M. P. Harold, *Appl. Catal., B*, 2019, **242**, 469–484.
44 C. R. Thomas, J. A. Pihl, V. Y. Prikhodko, M. K. Kidder, J. A. Lauterbach and T. J. Toops, *Catal. Commun.*, 2021, **156**, 106308.
45 C. Asokan, Y. Yang, A. Dang, A. B. Getsoian and P. Christopher, *ACS Catal.*, 2020, **10**, 5217–5222.
46 K. Khivantsev, C. G. Vargas, J. Tian, L. Kovarik, N. R. Jaegers, J. Szanyi and Y. Wang, *Am. Ethnol.*, 2021, **133**, 395–402.
47 T. Nakatsuji, M. Matsubara, J. Rouistenmäki, N. Sato and H. Ohno, *Appl. Catal., B*, 2007, **77**, 190–201.
48 S. Yasumura, T. Toyao, Z. Maeno and K. Shimizu, *ACS Catal.*, 2021, 12293–12300.
49 S. Yasumura, T. Kato, Y. Qian, T. Toyao, Z. Maeno and K. Shimizu, *J. Phys. Chem. C*, 2022, **126**, 19147–19158.
50 E. Ivanova and K. Hadjiivanov, *Phys. Chem. Chem. Phys.*, 2003, **5**, 655–661.
51 S. Maeda, Y. Harabuchi, M. Takagi, K. Saita, K. Suzuki, T. Ichino, Y. Sumiya, K. Sugiyama and Y. Ono, *J. Comput. Chem.*, 2018, **39**, 233–250.
52 M. Brändle and J. Sauer, *J. Am. Chem. Soc.*, 1998, **120**, 1556–1570.
53 H. Xia, *ACS Omega*, 2020, **5**, 9707–9713.
54 J. T. Yates, S. D. Worley, T. M. Duncan and R. W. Vaughan, *J. Chem. Phys.*, 1979, **70**, 1225–1230.
55 B. E. Hayden, A. King, M. A. Newton and N. Yoshikawa, *J. Mol. Catal. A: Chem.*, 2001, **167**, 33–46.

56 K. A. Almusaiteer and S. S. C. Chuang, *J. Phys. Chem. B*, 2000, **104**, 2265–2272.
57 S. Yasumura, Y. Qian, T. Kato, S. Mine, T. Toyao, Z. Maeno and K. Shimizu, *ACS Catal.*, 2022, **12**, 9983–9993.
58 S. Yasumura, Y. Qian, T. Toyao, Z. Maeno and K. Shimizu, *J. Phys. Chem. C*, 2022, **126**, 11082–11090.
59 S. Yasumura, C. Liu, T. Toyao, Z. Maeno and K. Shimizu, *J. Phys. Chem. C*, 2021, **125**, 1913–1922.